SMAR 2017 – Fourth Conference on Smart Monitoring,
Assessment and Rehabilitation of Civil Structures

SMAR 2017

Intermediate debonding on cracked steel beams reinforced with CFRP plates under fatigue

Massimiliano Bocciarelli[1], Pierluigi Colombi[1], Tommaso D'Antino[1] and Giulia Fava[1]

[1] ABC Department, Politecnico di Milano, Milan, Italy

ABSTRACT: Externally bonding by using Carbon Fibre Reinforced Polymers (CFRP) plates is often regarded as an effective technique to strengthen notched steel beams. On the other hand, intermediate debonding in the reinforced steel beam has a significant effect on fatigue crack propagation. Note that the fatigue load does not directly cause the debonding, but it may trigger crack propagation in the steel substrate, leading to the propagation of the debonded region. At first, the outcomes from an experimental campaign previously conducted at the Politecnico di Milano were considered. Then, analytical and numerical models were proposed to evaluate the strain distribution in the reinforcement at a given crack length. A good agreement was found among the analytical, numerical and experimental results in terms of strain distribution in the CFRP material.

1 INTRODUCTION

The use of Carbon Fibre Reinforced Polymers (CFRP) as reinforcing materials for retrofitting structural elements is nowadays considered as a suitable alternative to conventional techniques. This is true for concrete, masonry and even for timber structures. Studies have shown that external reinforcing with CFRP materials is an efficient technique for strengthening steel members (Zhao (2014)). In most of the available researches, CFRP reinforcements were applied on undamaged steel elements under both static tensile (plates) or bending (beams) load. In these cases, the load carrying capacity increased with a marginal stiffness increment. Besides, when CFRP materials were used to retrofit artificially damaged steel elements, under both static tensile (plates) and bending (beams) load, experimental results showed that the reinforcements were able to restore different levels of load carrying capacity and in some cases to increase them with respect to the original ones. Finally, CFRP repair of cracked steel elements (plates or beams) were found to significantly improve the fatigue life (Hu et al. (2016), Colombi et al. (2016)). This means that CFRP materials are really effective against fatigue problems as they reduce the stresses at the crack tip, the crack opening displacement and the effective stress range. CFRP materials are even more active if they are pre-stressed (Kianmofrad et al. (2017)). In this case, in fact, compressive stresses are introduced in the reinforced element, which additionally reduce the effective stress range and then enhance the fatigue life.

All the experimental outcomes confirmed that the bond between the composite material and the steel element is the weakest link of the strengthening technique. Several analytical (Deng et al. (2016)) and numerical models (Teng et al. (2015)) were then proposed in the literature to

investigate the stress concentration at the reinforcement end (end debonding) and at notch location (intermediate debonding) under static load. Debonding has also a detrimental effect in fatigue repaired steel elements since it reduces the fatigue life (Colombi et al. (2015), Colombi and Fava (2015)). Nonetheless, although debonding at notch location under static or fatigue load has a significant influence on the effectiveness of the CFRP strengthening, a limited number of research projects were performed in the literature.

1.1 Problem statement

CFRP reinforcement can effectively retrofit notched steel elements (plates and beams) under both static and fatigue load. In particular, under fatigue load the composite material reduces the stresses at the crack tip, the crack opening displacement and the effective stress range. It is then evident that the composite stiffness plays a very important role in the fatigue retrofit of cracked steel elements. High-stiffness composite materials result, in fact, in a significant decrease of the stresses at the crack tip, the crack opening displacement and of the effective stress range. On the other hand, the notch introduces stress concentrations, which eventually result in debonding at the interface. Also, it was clearly shown that the presence of a region where the materials interface is damaged or debonded has a significant influence on the fatigue life (Colombi et al. (2015), Colombi and Fava (2015)). As well known, the fatigue crack propagation is driven by the stress intensity factor range at the crack tip. In the literature, a simple formula was proposed to evaluate the stress intensity factor of unreinforced cracked I-beams. It was based on elementary beam theory and was extended more recently to cover CFRP reinforced cracked I-beams (Ghafoori et al. (2011)). The composite materials, in fact, introduce a compressive force in the steel beam that is clearly not applied at the centroid of the cracked section. Thus, an additional bending moment should be introduced to take into account such load eccentricity. The above mentioned compressive force has then a strong influence on the stress intensity factor evaluation of the cracked steel beam. Analytical or numerical models for the estimation of the axial force in the composite material are then mandatory for a reliable estimation of the fatigue life of retrofitted steel beams.

1.2 Scope of the research

In this paper, I-shaped simple supported steel beams tested under fatigue load (four-point bending) are considered (Colombi and Fava (2015)). The main aim of this work is to discuss the effect of debonding on the axial force in the composite material. Recently, an analytical model was presented (Colombi and Fava (2016)) but it provides just an estimation of the axial force for long crack lengths. Besides, a simplified numerical model (FE model) was proposed to validate the analytical results. A more refined FE analysis that employs a damage cohesive interface is then suggested in this work to provide a more detailed estimation of the axial force in the composite material. Numerical analyses are performed for given crack lengths and the effect of fatigue load on debonding was disregarded. In Zheng and Dawood (2017), in fact, it was observed that the fatigue load does not directly influence debonding. Somewhat, fatigue load produces crack propagation in the steel element, which results in debonding propagation. The proposed numerical model is validated by comparing the numerical axial strain in the composite material to the experimental outcomes presented in Colombi and Fava (2015).

2 EXPERIMENTAL EVIDENCE

2.1 Test program

Nine cracked steel beams were reinforced in Colombi and Fava (2015) by using pultruded CFRP strips and tested under fatigue load to analyze crack induced debonding and its effect on fatigue crack propagation (see Figure 1a). I-shaped steel beams (IPE 120 according to EN 10025) were artificially notched at the mid-span section through the tension flange and a portion of the web (see Figure 1b). At first, unreinforced notched beams were loaded under fatigue (6-15 kN) to produce a pre-crack in the web with a length equal to 20 mm. Then the beams were reinforced with CFRP strips prior to start the fatigue tests.

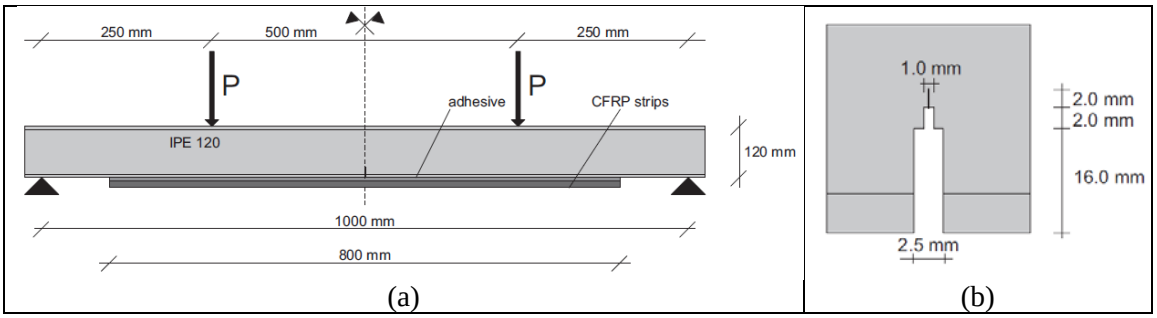

Figure 1. Specimen geometry: (a) experimental beam geometry and (b) notch details (not to scale).

The beam steel type was S275J0, according to standard EN 10025. Based on tensile tests, the mean yielding stress and tensile strength were 330 MPa and 444 MPa, respectively. A Young's modulus of 208 GPa was measured. As in real applications, the beams were strengthened using pultruded CFRP strips (Sika CarboDur M614), with a thickness of 1.4 mm, a width of 60 mm and a length of 800 mm. The nominal values of the Young's modulus and tensile strength were greater than 200 GPa and 2800 MPa, respectively. The reinforcement Young's modulus was assumed equal to 195 GPa. The CFRP strips were bonded using a two-component thixotropic epoxy resin (Sikadur 30) with an adhesive thickness of 2.5 mm. For specimens reinforced with two CFRP layers, the inner CFRP strip was bonded to the beam by using Sikadur 30 epoxy resin, while a less viscous epoxy (Sikadur 330) was used to bond the outer CFRP strip to the inner one. In this case the adhesive thickness between the inner and outer reinforcement strips was equal to 1 mm.

2.2 Fatigue tests and recording equipment

All beams were subjected to four-point bending load over a simply supported span of 1000 mm (see Figure 1). A special test rig was designed to perform the experimental tests and a spreader beam was used to distribute the load to the beam. The crack growth was measured using a travelling microscope. Specimen details are shown in Table 1, where a_i and a_f are the initial and final crack length, t_c is the CFRP thickness and ΔF is the load range.

Strain gauges were positioned on the CFRP strips of beams B04, B06, B07 and B09 (see Figure 2a), to investigate the tensile strain distribution and to monitor the progressive debonding propagation of the CFRP close to the notch. In the case of reinforcements made of two CFRP layers, debonding may also occur at the interface between the two reinforcement layers, but this was not checked experimentally. Nonetheless, strain gauges measurements were useful to

examine the debonding shape effects on the crack propagation curves and to analyze the mutual influence of the fatigue crack propagation and the reinforcement debonding.

Table 1. Test layout

Spec.	a_i (mm)	t_c (mm)	ΔF (kN)	a_f (mm)
B01	20	/	6–15 (10 Hz)	60
B02	20	1.4 (1 layer)	6–15 (10 Hz)	20
B03	20	1.4 (1 layer)	28–70 (3 Hz)	60
B04	20	1.4 (1 layer)	28–70 (3 Hz)	60.9
B05	20	2.8 (2 layers)	28–70 (3 Hz)	60.4
B06	20	2.8 (2 layers)	28–70 (3 Hz)	60.9
B07	20	2.8 (2 layers)	28–70 (3 Hz)	60.4
B08	20	2.8 (2 layers)	28–70 (3 Hz)	60.2
B09	20	2.8 (2 layers)	28–70 (3 Hz)	35

For specimens B04 and B07, referring to the strain gauges positions reported in Figure 2a, the CFRP strain distributions for increasing crack lengths are shown in Figure 2b and 2c. Distributions are symmetric with respect to the mid-span, but the strains tend to spread as the crack length increases, due to the progressive debonding. For specimen B04, the strain profile showed a plateau up to approximately 50 mm from the mid-span, indicating the presence of a debonded area close to the crack. This phenomenon is less evident but also observed in beam B07 that was reinforced with two CFRP strips.

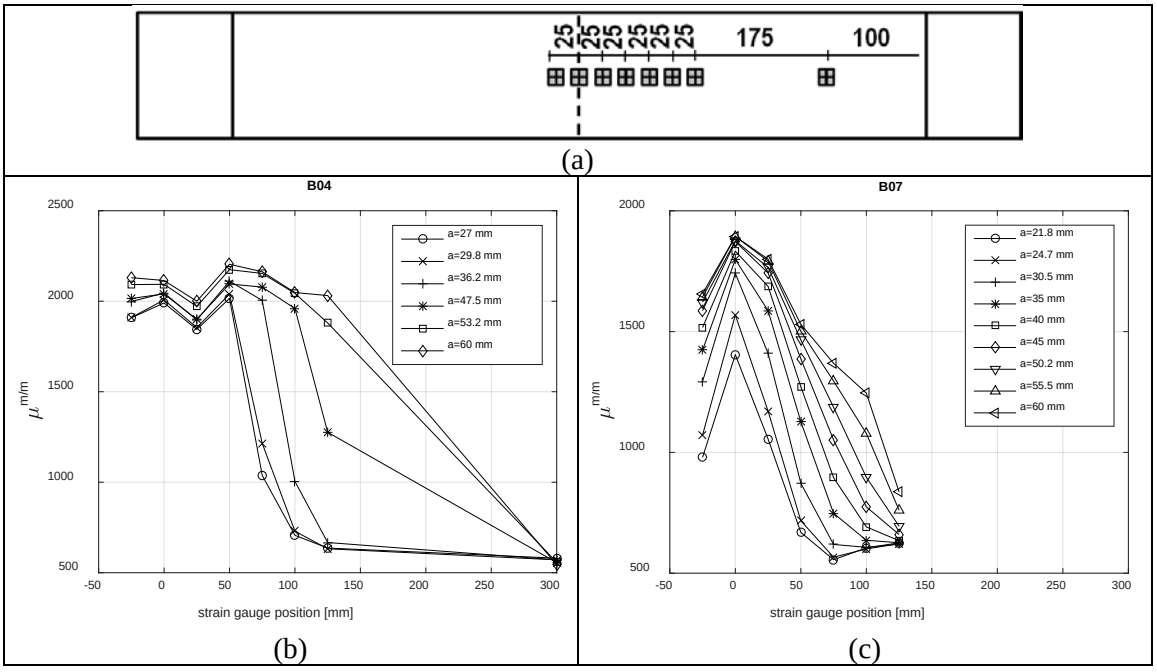

Figure 2. (a) Strain gauge layout, (b) Strain gauge measurement in specimen B04 (1 CFRP layer), (c) Strain gauge measurement in specimen B07 (2 CFRP layers).

3 ANALYTICAL MODEL

In this section, the analytical model proposed in Colombi and Fava (2016) for the estimation of the axial force in the reinforcement for long crack lengths is summarized. A simplified one-parameter shear lag model (that is, no peeling stresses are considered) is used to perform the stress analyses. In this work a cohesive model is associated with the interface between the CFRP material and the steel beam. In particular, the following exponential bond-slip law is often adopted in the literature (Bocciarelli et al. (2016)):

$$\tau = \delta \frac{\tau_p}{\delta_p}\left[\exp\left(1-\frac{\delta}{\delta_p}\right)\right] \tag{1}$$

where τ_p is the maximum shear stress and δ_p is the relative displacement at τ_p. The bond-slip law is depicted in Figure 3 where G_c is the area under the bond-slip law (fracture energy). In this case one has for the fracture energy $G_c = e\delta_p\tau_p$ and the initial slope $p_{ini} = e\tau_p/\delta_p$. Note that in the elastic stage the stiffness of the interface should be equal to the shear deformability of the adhesive layer, therefore $p_{ini} = G_a/t_a$, where G_a and t_a are the shear modulus and the thickness of the adhesive layer. Finally, for the above exponential bond-slip law the fracture energy is equal to $G_c = e^2\tau_p^2 t_a/G_a$ as function of the maximum interface shear stress and of the adhesive properties. In Cornetti et al. (2015), a nonlinear softening bond-slip law was used to define the equilibrium path and the relevant maximum end debonding load. Also for intermediate debonding of notched beams, analytical models with a nonlinear bond-slip law were developed (Wang (2006)). In both cases, this resulted in a quite complicated procedure even for a very simple geometry and load configuration.

In Bocciarelli et al. (2016), a simplified procedure was introduced to investigate the end debonding of undamaged steel beams strengthened with CFRP materials under a general load condition and structural configuration. The main idea was to substitute the nonlinear bond-slip law (see Figure 3a) with an equivalent linear bond-slip one:

$$\tau = k\delta \tag{2}$$

where k is the slope of the linear bond-slip law (see Figure 3b). In this case one has $G_c = \delta_p\tau_p/2$ and $k = G_a/t_a$. Finally, for the linear bond-slip law the fracture energy is equal to $G_c = \tau_p^2 t_a/2G_a$ as function of the maximum interface shear stress and of the adhesive properties. If the two fracture energies are equal, the same debonding load is achieved, as shown in Bocciarelli et al. (2016) for end debonding. This concept was used in Colombi and Fava (2016) to investigate the intermediate debonding observed in fatigue tests. Under standard basic hypotheses, the following expression for the maximum shear stress τ_{max} in the adhesive layer was calculated as function of the applied bending moment, M, and the axial force, N_{c0}, in the composite material in the notched section:

$$\tau_{\max} = \frac{\lambda}{b_f}\left(N_{c0} - \frac{M}{E_s W_s}E_f A_f\right) \tag{3}$$

where E_f and $A_f=t_f b_f$ are the Young's modulus and the area of the composite material, respectively, while E_s and W_s are the Young's modulus and the resistance modulus of the steel substrate, respectively. In Eq. (3), one also has $\lambda = \sqrt{G_a/E_f t_f t_a}$. At debonding $\tau_{max}=\tau_p$ and

then the following relationship holds for the axial force in the composite material at debonding, $N_{c,deb}$, as function of the fracture energy G_c:

$$N_{c,deb} = b_f \sqrt{2G_c E_f t_f} + MA_f E_f / E_s W_s \tag{4}$$

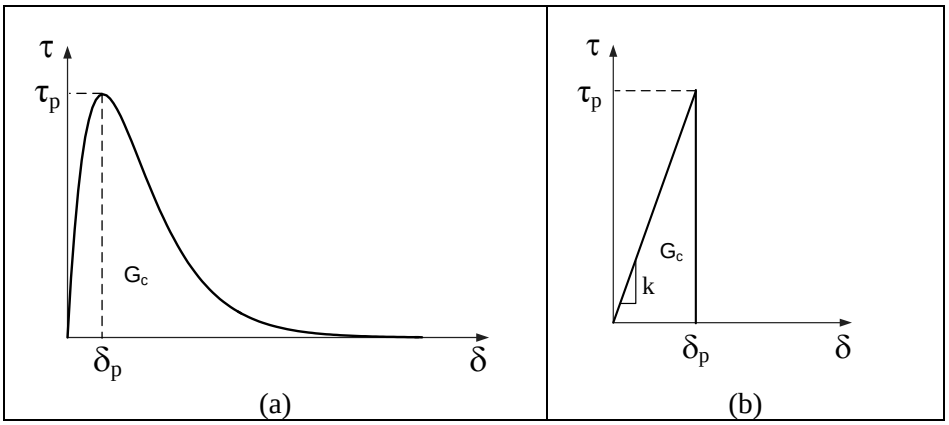

Figure 3. Exponential (a) and linear (b) bond-slip law.

4 NUMERICAL MODELLING

The strain in the CFRP composite applied to strengthen the steel I-beams described in Colombi and Fava (2016) was investigated by means of 3D FE numerical models using the software Abaqus. The geometry of the steel beams was reproduced using shell elements located at the mid-plane of the I-beam flanges and web. The crack in the steel beam flange was just modeled considering two different shell elements. In the steel web a partition was generated to represent the crack and separate nodes on elements on each side of the crack were created by defining a seam. The CFRP composite was modeled as a shell element with the same geometry of the pultruded strips employed experimentally and was bonded to the soffit of the steel I-beam through a non-linear damage cohesive contact law. The initial behavior of the contact interface is linear and is defined by the slopes K_{nn}, K_{ss}, and K_{tt} associated with the normal (subscript *nn*) and the two shear directions (subscript *ss* and *tt*). When the quadratic stress criterion (Simulia (2016)) is satisfied, damage occurs and the behavior of the interface becomes non-linear. In the numerical models employed, damage was defined for discrete slip values to reproduce the selected bond-slip law.

Two distinct contact interfaces were considered in the numerical analyses. The first one was located at the reinforcement/steel interface. In this case the exponential bond-slip law described in Eq. (1) is adopted. The second one (if present) was inserted at the interface between the two reinforcement layers. The interface parameters were calibrated by an inverse batch deterministic procedure. With reference to the reinforcement/steel interface, a fracture energy of 0.34 N/mm was employed. Besides, a maximum shear stress τ_p=5.20 MPa and a relative displacement at maximum shear stress δ_p=0.024 mm were adopted. Then, an adhesive (Sikadur 30) shear modulus of G_a=1460 MPa was selected, resulting in an initial stiffness p_{ini}=584 N/mm^3. Finally, with reference to the interface between the two reinforcement layers, a linear bond-slip law as in Eq. (2) was chosen with an adhesive (Sikadur 330) shear modulus G_a=760 MPa, resulting in an interface stiffness k=760 N/mm^3. In this case, no interface damage was observed and then no other interface parameters are required. Note that the numerical values listed above do not match the ones suggested in the literature (Fawzia et al. (2010), Teng et al. (2015)) but they fit

with a reasonable degree of accuracy the experimental outcomes and in this sense they reflect the specific specimen preparation.

In the mesh, 4-node reduced integration shell elements were used to discretize the steel beam (9176 square elements with edge of approximately 6 mm) and the CFRP strip (3060 square elements with edge of approximately 3 mm). The FE analyses were carried out under force control using an implicit Newton-Raphson solver scheme. The beams were loaded until an applied force of 70 kN was attained, which is equal to the maximum applied force adopted for the experimental fatigue tests.

5 RESULTS AND DISCUSSION

Five numerical models with different ratios between crack length and cross-section depth *a/h*, namely 0.167, 0.2, 0.3, 0.4 and 0.5, were studied. For each of the normalized crack lengths, the FEM described in the previous section was implemented to evaluate the strain distribution in the reinforcement layer.

With reference to a single reinforcement layer (specimen B04), debonding was observed from the beginning of the test and then the axial strain in the reinforcement layer is constant (see Figure 4b). In this case, Eq. (4) provides a longitudinal strain ε_c=2228 mm/m, which reasonably agrees with the experimental outcomes (see Figure 4b).

On the other hand, with reference to beam specimens reinforced with two layers (specimens from B06 to B09), results for short crack lengths (Figure 4a) clearly show that the strain redistribution is mainly confined in the inner reinforcement layer close to the steel beam while the outer one is marginally involved. This is not the case for large crack lengths where both layers contribute significantly to the load carrying capacity. Besides, for large crack lengths (*a/h* greater than 0.3), the longitudinal strain is almost constant (see Figure 4b) and approximately equal to the longitudinal strain at debonding. This limit value was soundly estimated by using Eq. (4) and it results in a longitudinal strain ε_c=1739 mm/m (Figure 4b).

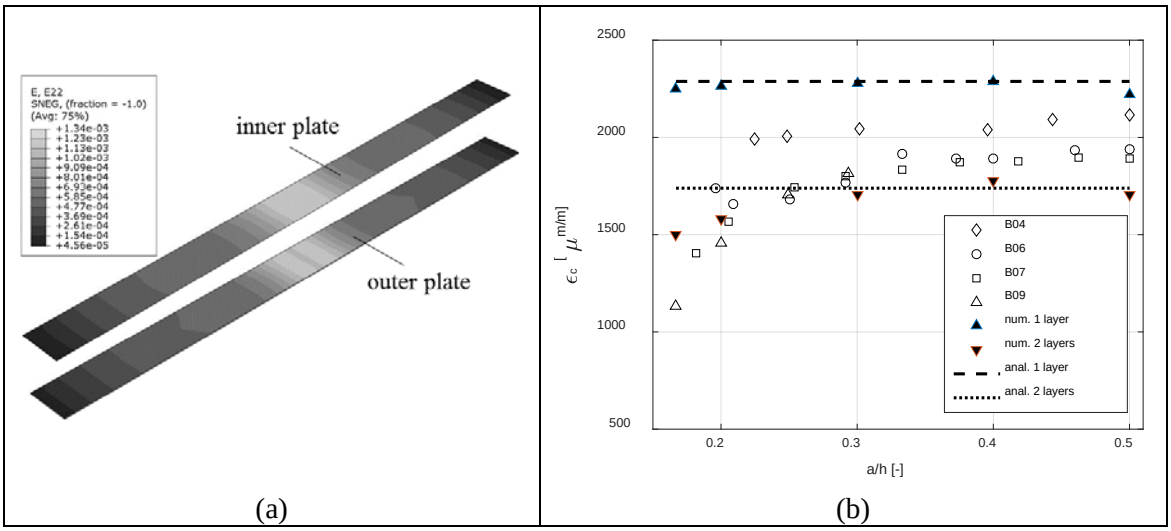

Figure 4. Finite element contour of the longitudinal strain distribution for *a/h*=0.167 (a) and (b) longitudinal strain as function of the normalized crack length *a/h* from both the numerical and analytical model compared to experimental results.

6 CONCLUSIONS

Numerical and analytical results illustrate that for a single reinforcement layer debonding is present at the reinforcement/steel interface due to the high stress concentration. This is in agreement with the experimental outcomes.

On the other hand, experimental results showed that the fatigue crack growth of steel beams reinforced with two layers is a complex phenomenon which is influenced by different interfaces behavior (Colombi and Fava, (2015)). In detail, for short crack lengths the stress redistribution involves just one reinforcement layer, while for large crack lengths the stress redistribution affects both the reinforcement layers. This is correctly captured by the proposed numerical model as shown in Figure 4b. Besides, in this case the proposed analytical model also provides an estimation of the longitudinal strain for large crack length. Researches are in progress to improve the analytical model to capture the behavior of short crack lengths as well.

7 REFERENCES

Zhao, XL. 2014. *FRP-strengthening metallic structures*. CRP Press, Taylor & Francis Group, Boca Raton, London, New York.

Hu, L.L., and X.L. Zhao, 2016, Fatigue behavior of cracked high-strength steel plates strengthened by CFRP sheets. *Journal of Composites for Construction*, 20(6): 04016043.

Colombi, P., and G. Fava, 2016, Fatigue crack growth in steel beams strengthened by CFRP strips. *Theoretical and Applied Fracture Mechanics*, 85: 173-182.

Kianmofrad, F., E. Ghafoori, M.M. Elyasi, M. Motavalli, and M. Rahimian, 2017, Strengthening of metallic beams with different types of pre-stressed un-bonded retrofit systems. *Composite Structures*, 159: 81-95.

Colombi, P., G. Fava and L. Sonzogni, 2015, Fatigue crack growth in CFRP strengthened steel plates. *Composites: Part B*, 72: 87-96.

Colombi, P., and G. Fava, 2015, Experimental study on the fatigue behavior of cracked steel beams repaired with CFRP plates. *Engineering Fracture Mechanics*, 145: 128-142.

Deng, J., Y. Jia and H. Zheng, 2016, Theoretical and experimental study on notched steel beams strengthened with CFRP plate. *Composite Structures*, 136: 450-459.

Teng, J.C., D. Fernando, and T. Yu, 2015, Finite element modelling of debonding failures in steel beams flexurally strengthened with CFRP laminates. *Engineering Structures*, 86: 213-224.

Ghafoori, E., and M. Motavalli, 2011, Analytical calculation of stress intensity factor of cracked steel I-beams with experimental analysis and 3D digital image correlation measurements. *Engineering Fracture Mechanics*, 78 (18): 3226-3242.

Zheng, B., and M. Dawood, 2017, Fatigue crack growth analysis of steel elements reinforced with shape memory alloy (SMA)/fiber reinforced polymer (FRP) composite patches. *Composite Structures*, 164: 158-169.

EN 10025. 2004. Hot rolled products of structural steels. General technical delivery conditions.

Bocciarelli, M., P. Colombi, G. Fava, and L. Sonzogni, 2016, Energy-based analytical formulation for the prediction of end debonding in strengthened steel beams. *Composite Structures*, 153: 212-221.

Cornetti P., M. Corrado, L. De Lorenzis, and A. Carpinteri, 2015, An analytical cohesive crack modeling approach to the edge debonding failure of FRP-plated beams. *International Journal of Solids and Structures*; 53: 92-106.

Wang, J., 2006, Cohesive zone model of intermediate crack-induced debonding of FRP-plated concrete beams. *International Journal of Solids and Structures*; 43: 6630-6648.

Simulia. 2016. *Abaqus 6.13 Extended Functionality Online Documentation* (generated January 15, 2016).

Fawzia S., X.L. Zhao, and R. Al-Mahaidi, 2010, Bond–slip models for double strap joints strengthened by CFRP. *Composite Structures*, 92(9):2137–45.